

## Total fusion of ${}^9\text{Be}+{}^9\text{Be}$ at $E({}^9\text{Be})=35\text{--}55\text{ MeV}$

A. R. Omar and J. S. Eck

*Department of Physics, Kansas State University, Manhattan, Kansas 66506*

T. R. Ophel and J. R. Leigh

*Department of Nuclear Physics, Australian National University, Canberra, ACT 2600, Australia*

(Received 5 July 1984)

Fusion cross sections for the  ${}^9\text{Be}+{}^9\text{Be}$  system have been measured by detecting the evaporation residues using a gas-ionization—surface-barrier  $\Delta E$ - $E$  detector at  ${}^9\text{Be}$  bombarding energies of 35–55 MeV in 5 MeV steps. The ratios of the measured total fusion cross section to the total reaction cross section calculated using optical model parameters which fit the elastic scattering cross sections were found to be very small compared to the same results obtained from fusion studies of  ${}^9\text{Be}+{}^{28}\text{Si}$  and  ${}^9\text{Be}+{}^{40}\text{Ca}$  systems. This behavior is attributed to the high probability for breaking up of  ${}^9\text{Be}$  before the critical distance of fusion is reached.

### INTRODUCTION

Fusion studies<sup>1–4</sup> of systems involving the weakly bound  ${}^9\text{Be}$  projectile, such as  ${}^9\text{Be}+{}^{28}\text{Si}$  and  ${}^9\text{Be}+{}^{40}\text{Ca}$ , have shown that even at low energies [ $E({}^9\text{Be})\sim 30\text{ MeV}$ ] the ratio of the total fusion cross section to the total reaction cross section is relatively small compared to fusion reactions involving carbon, nitrogen, or oxygen projectiles and similar target nuclei. This is attributed to the ease with which the  ${}^9\text{Be}$  dissociates into smaller fragments. Optical model analysis of the elastic scattering indicates that the absorption potential is strong and diffuse,<sup>5</sup> which means that nonelastic processes (including dissociation) set in at a larger distance of separation between the  ${}^9\text{Be}$  and the target nucleus than in cases of heavier projectiles ( $A\geq 12$ ).

Another anomalous behavior which occurs for  ${}^9\text{Be}$  interactions is the need to reduce the calculated double folding potential that utilizes a realistic effective nucleon-nucleon interaction in order to obtain a successful fit to the elastic scattering cross sections and may further indicate the strong influence of breakup channels on the nuclear interaction.<sup>5–12</sup> To date, fusion studies have been carried out which involve the weakly bound  ${}^9\text{Be}$  projectile interacting with a strongly bound target (either  ${}^{28}\text{Si}$  or  ${}^{40}\text{Ca}$ ), and the anomalous behavior observed has been attributed to the properties of the weakly bound  ${}^9\text{Be}$ . In the present study the interaction of two weakly bound  ${}^9\text{Be}$  nuclei is carried out in an effort to shed more light on the interaction of weakly bound nuclei. The experimental details are outlined in Sec. II, the results and a discussion of the results are presented in Sec. III, and the conclusions are given in Sec. IV.

### EXPERIMENTAL

The  ${}^9\text{Be}$  beam was extracted from a sputtering ion source and was accelerated by the Australian National University (ANU) 14UD Pelletron tandem accelerator. The target consisted of self-supporting  ${}^9\text{Be}$  foils ( $\sim 100$

$\mu\text{g}/\text{cm}^2$ ) with a trace amount of gold evaporated onto it. A ninefold ionization-chamber—surface-barrier detection system was used to detect the evaporation residues. A more detailed account of the instrumentation is given elsewhere.<sup>13</sup>

The data were recorded in the event mode where each event consisted of an  $E$ , a  $\Delta E$ , and a detector identification signal. The events were recorded on magnetic tape for later off-line analysis. In order to record all evaporation residues simultaneously in an efficient manner, the  $E$  signal was fed through both a high gain and a low gain amplifier. The gains of the two  $E$  signal amplifiers were scaled with energy so as to maintain the same relative threshold. The typical low gain and high gain spectra of  ${}^9\text{Be}+{}^9\text{Be}$  evaporation residues are shown in Fig. 1.

The fusion cross section angular distributions for  ${}^9\text{Be}+{}^9\text{Be}$  were obtained by summing the yields of evaporation residues with  $Z\geq 4$ . The absolute cross sections were obtained by normalizing the fusion cross sections to the elastic scattering cross sections. The angular distributions for fusion products described by

$$\frac{d\sigma_{\text{fus}}}{d\theta} = 2\pi \sin\theta \frac{d\sigma_{\text{fus}}}{d\Omega}$$

are shown in Fig. 2. The total fusion cross section at a given energy was obtained by summing the area under the angular distribution. The total fusion cross sections as a function of energy are shown in Fig. 3. Total reaction cross sections were calculated using the optical model parameters which yielded good fits to the elastic scattering cross sections.<sup>14</sup> These parameters are  $V_0=12.0\text{ MeV}$ ,  $r_0=1.2\text{ fm}$ ,  $a_0=0.73$ ,  $W=20.0\text{ MeV}$ ,  $r_w=1.3\text{ fm}$ , and  $a_w=0.75\text{ fm}$ . In order to facilitate comparison with the total fusion cross sections, the total reaction cross sections as a function of energy are also shown in Fig. 3. The fusion cross sections are much lower than the total reaction cross sections. At  $E({}^9\text{Be})=35\text{ MeV}$  the fusion cross section is  $\sim 12\%$  of the total reaction cross section and decreases as the energy increases, until at  $E({}^9\text{Be})=55$

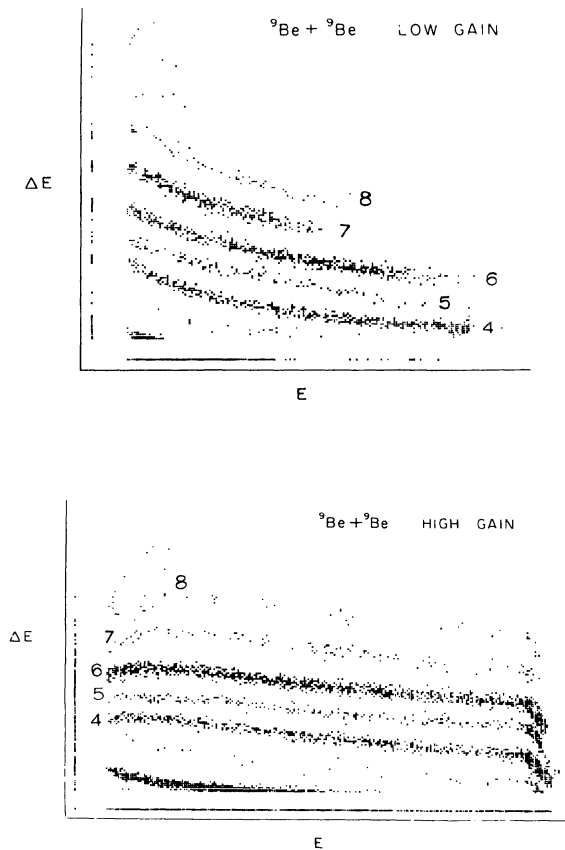


FIG. 1. Energy loss,  $\Delta E$ , as a function of energy  $E$  for reaction products from  ${}^9\text{Be}+{}^9\text{Be}$  at  $E({}^9\text{Be})=40$  MeV. Top spectrum is for a low gain setting on  $E$  amplifier. Bottom spectrum is for a high gain setting on  $E$  amplifier. Number marking each curve is the atomic number,  $Z$ , of the corresponding evaporation residues.

MeV it contributes only  $\sim 1.5\%$  of the total reaction cross section.

Fusion studies of  ${}^9\text{Be}+{}^{40}\text{Ca}$  and  ${}^9\text{Be}+{}^{28}\text{Si}$  have shown that  $\sigma_{\text{fus}}/\sigma_{\text{reac}} \sim 0.3\text{--}0.5$  for the same bombarding energy range.<sup>1,3</sup> This low ratio is attributed to the fact that the

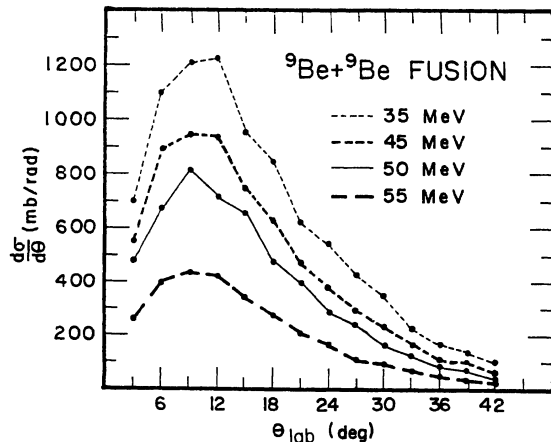


FIG. 2. Angular distributions of total evaporation residues with  $Z \geq 4$  for the  ${}^9\text{Be}+{}^9\text{Be}$  interaction at the various bombarding energies.

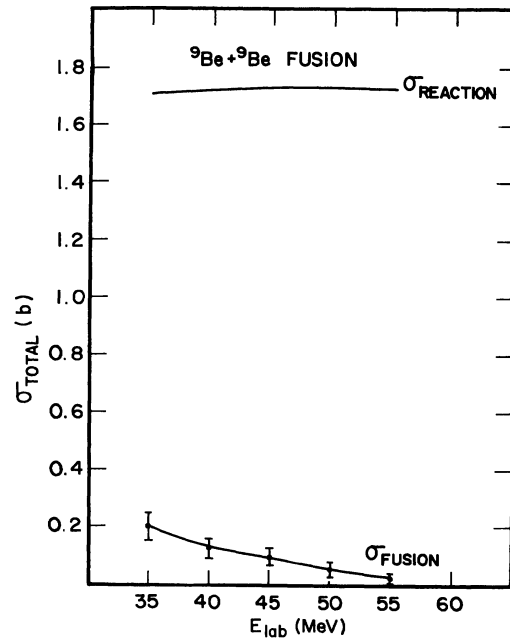


FIG. 3. Total fusion cross sections as a function of energy. Also shown is the total reaction cross section as a function of energy which was calculated using the optical model and parameters which yielded fits to the elastic scattering angular distributions.

${}^9\text{Be}$  projectile is spatially large and breaks up into  $2\alpha+n$  before the critical distance for fusion is reached. In the case of the  ${}^9\text{Be}+{}^9\text{Be}$  fusion, in addition to the ease of breakup of the  ${}^9\text{Be}$ , the present definition of fusion in terms of evaporation residues with  $Z \geq 4$  may be inadequate to define fusion. When a highly excited  ${}^{18}\text{O}$  compound system is formed, it can very likely break up into 4  $\alpha$  particles or even sequentially emit  $\alpha$  particles such that the final products of the reaction are 4  $\alpha$ 's and 2 neutrons. Thus, even if a compound system were formed (i.e., fusion occurred), it would not be included in the fusion cross sec-

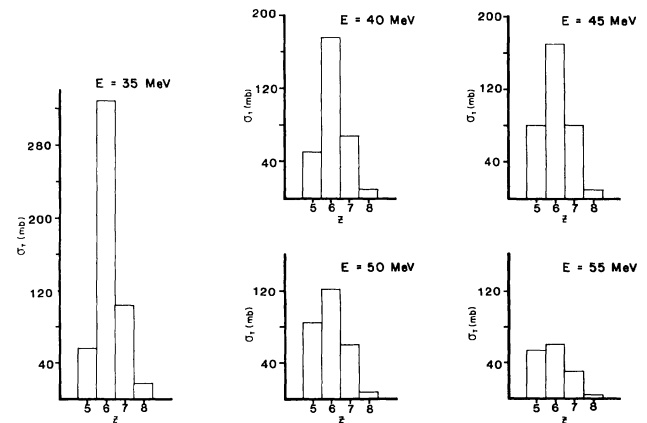


FIG. 4. Total cross section of the various evaporation residues from  ${}^9\text{Be}+{}^9\text{Be}$  interaction at the various  ${}^9\text{Be}$  bombarding energies. Note the decrease in the dominance of the  $Z=6$  residue as energy increases.

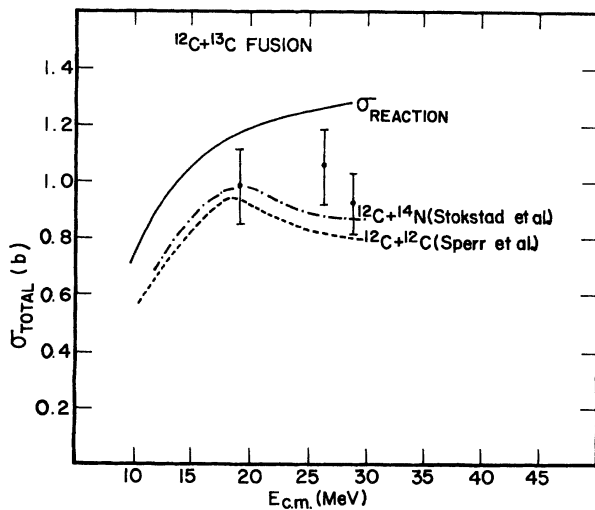


FIG. 5. Total fusion cross section for  $^{12}\text{C}+^{13}\text{C}$  as a function of energy (dots with error bars). Also shown are  $^{12}\text{C}+^{14}\text{N}$  and  $^{12}\text{C}+^{12}\text{C}$  fusion cross sections and the total reaction cross section for  $^{12}\text{C}+^{13}\text{C}$  calculated from the optical model using optical model parameters which fit the elastic scattering angular distributions.

tions as determined by summing the evaporation residues. This may possibly explain the lowering of  $\sigma_{\text{fus}}/\sigma_{\text{reac}}$  for  $^9\text{Be}+^9\text{Be}$  to  $\sigma_{\text{fus}}/\sigma_{\text{reac}} \sim 0.1$ .

In Fig. 4 are shown the relative production of the different evaporation residues at a given energy. At  $E_{\text{lab}}=35$  MeV the fusion reaction is dominated by the cross section for production of the carbon evaporation residues. At  $E_{\text{lab}}=55$  MeV the dominance of the carbon residue contribution to the fusion cross sections is no longer so well pronounced. This can be interpreted by assuming that at  $E_{\text{lab}}=35$  MeV the compound system still retains the  $\alpha$  particle configurations of the interacting  $^9\text{Be}$  nuclei while at higher energies this feature begins to disappear and the compound nucleus has a structure more reminiscent of an equilibrated collection of neutrons and protons.

Fusion cross sections for the system  $^{13}\text{C}+^{12}\text{C}$  were also measured at  $E(^{13}\text{C})=40, 55,$  and  $60$  MeV using a  $20 \mu\text{g}/\text{cm}^2$  self-supporting target and the same experimental setup as used for the  $^9\text{Be}+^9\text{Be}$  measurements. The elastic scattering cross section angular distributions were mea-

sured simultaneously with the  $^{13}\text{C}+^{12}\text{C}$  evaporation residues. The absolute cross sections were obtained by normalizing to the elastic scattering. Total fusion cross sections were obtained by summing all evaporation residues with  $Z \geq 6$  and integrating over angle. The total fusion cross sections are shown in Fig. 5 along with the total fusion cross sections<sup>15,16</sup> for  $^{12}\text{C}+^{14}\text{N}$  and  $^{12}\text{C}+^{12}\text{C}$  and the total reaction cross section obtained from optical model calculations using the same parameters which fit the elastic scattering angular distributions. The optical parameters used were  $V=86.6$  MeV,  $r_0=1.084$  fm,  $a_0=0.586$  fm,  $W=9.563$  MeV,  $r_w=1.263$  fm, and  $a_w=0.329$  fm, and were taken from the work of Westfall and Zaidi.<sup>17</sup> It can be seen that the fusion cross sections for  $^{13}\text{C}+^{12}\text{C}$  are comparable in magnitude to those for  $^{12}\text{C}+^{14}\text{N}$  and  $^{12}\text{C}+^{12}\text{C}$  at the same center-of-mass energies. The total reaction cross section for  $^{12}\text{C}+^{13}\text{C}$  is larger than the measured fusion cross section by about 20–25% in the energy range of  $E_{\text{c.m.}}=20$ – $30$  MeV. Thus the fusion cross sections involving  $^{13}\text{C}$  projectiles are similar to those for other heavy ions ( $A \geq 12$ ). Although we can think of  $^{13}\text{C}$  as a  $^{12}\text{C}$  nucleus with a loosely bound neutron, the differences observed between reactions and scattering of  $^9\text{Be}$  from those of  $^{13}\text{C}$  are attributable to the loose binding of the  $\alpha$  particles in  $^9\text{Be}$  or conversely the tight binding of the  $\alpha$  particles comprising the  $^{12}\text{C}$  core in  $^{13}\text{C}$ .

## CONCLUSION

Fusion reaction cross sections for  $^9\text{Be}+^9\text{Be}$  have been measured and compared with total reaction cross sections obtained from optical model calculations.  $\sigma_{\text{fus}}/\sigma_{\text{reac}}$  decreases from 12% at  $E_{\text{lab}}=35$  MeV to 1.5% at 55 MeV. The observed evaporation residue spectrum following the fusion of  $^9\text{Be}+^9\text{Be}$  is dominated by the contribution of  $^{12}\text{C}$  at 35 MeV. As energy increases the relative contribution of  $^{12}\text{C}$  to the evaporation residue spectrum decreases considerably. These results have been interpreted in terms of the loosely bound  $\alpha$ -particle structure of the  $^9\text{Be}$  nucleus. The magnitude of the fusion cross section of  $^9\text{Be}+^9\text{Be}$  is, however, quite different from that of  $^{13}\text{C}+^{12}\text{C}$ , although in both cases the interacting nuclei have a strong  $\alpha$ -particle-like structure. This difference is attributed to the weak binding of  $^9\text{Be}$ .

<sup>1</sup>J. S. Eck, J. R. Leigh, T. R. Ophel, and P. D. Clark, Phys. Rev. C 21, 2352 (1980).  
<sup>2</sup>K. Bodek, M. Hugi, J. Lang, R. Müller, E. Ungricht, K. Janowski, W. Zipper, L. Jarczyk, A. Strzalkowski, G. Willim, and H. Witala, Nucl. Phys. A339, 353 (1980).  
<sup>3</sup>J. S. Eck, A. R. Omar, J. R. Leigh, and T. R. Ophel, Phys. Rev. C 27, 1807 (1983).  
<sup>4</sup>M. Hugi, J. Lang, R. Müller, E. Ungricht, K. Bodek, L. Jarczyk, A. Magiera, A. Strzalkowski, and G. Willim, Nucl. Phys. A368, 173 (1981).  
<sup>5</sup>J. S. Eck, T. R. Ophel, P. D. Clark, and D. C. Weissner, Nucl. Phys. A334, 519 (1980).

<sup>6</sup>G. R. Satchler and W. G. Love, Phys. Rep. 55C, 183 (1979).  
<sup>7</sup>R. Balzer, M. Hugi, B. Kamys, J. Lang, R. Miller, E. Ungricht, and J. Untermahrer, Nucl. Phys. A293, 518 (1977).  
<sup>8</sup>G. R. Satchler and G. W. Love, Phys. Lett. 65B, 415 (1976).  
<sup>9</sup>I. J. Thompson and M. A. Nagarajan, Phys. Lett. 106B, 163 (1981).  
<sup>10</sup>M. A. Nagarajan, I. J. Thompson, and R. C. Thompson, Nucl. Phys. A385, 525 (1982).  
<sup>11</sup>V. Hnizdo, K. W. Kemper, and J. Szmakowski, Phys. Rev. Lett. 46, 590 (1981).  
<sup>12</sup>M. S. Zisman, J. G. Cramer, D. A. Goldberg, J. W. Watson, and R. M. DeVries, Phys. Rev. C 21, 2398 (1980).

- <sup>13</sup>T. R. Ophel, W. Galster, D. J. Hinde, and J. R. Leigh, Nucl. Instrum. Methods **193**, 507 (1982).
- <sup>14</sup>A. R. Omar, J. S. Eck, J. R. Leigh, and T. R. Ophel, Phys. Rev. C **30**, 896 (1984).
- <sup>15</sup>P. Sperr, T. H. Braid, Y. Eisen, D. G. Kovar, F. W. Prossner, Jr., J. P. Schiffer, S. L. Tabor, and S. Vigdor, Phys. Rev. Lett. **37**, 321 (1976).
- <sup>16</sup>R. G. Stokstad, J. Gomez del Campo, J. A. Biggerstaff, A. H. Snell, and P. H. Stelson, Phys. Rev. Lett. **36**, 1529 (1976).
- <sup>17</sup>W. D. Westfall and S. A. Zaidi, Phys. Rev. C **14**, 610 (1976).